Journal of Magnetic Resonance 193 (2008) 54–62

Contents lists available at ScienceDirect

Journal of Magnetic Resonance

journal homepage: www.elsevier.com/locate/jmr

Measurement of the ^{14}N nuclear quadrupole resonance frequencies by the solid effect

J. Seliger [a,b,*], V. Žagar [a]

[a] "Jozef Stefan" Institute, Jamova 39, 1000 Ljubljana, Slovenia
[b] University of Ljubljana, Faculty of Mathematics and Physics, Department of Physics, Jadranska 19, 1000 Ljubljana, Slovenia

ARTICLE INFO

Article history:
Received 22 January 2008
Revised 10 April 2008
Available online 1 May 2008

Keywords:
N-14
Quadrupole resonance
Double resonance
Histamine
Quinolinic acid

ABSTRACT

^{1}H–^{14}N nuclear quadrupole double resonance using magnetic field cycling between high and low magnetic field and solid effect in the low magnetic field is analyzed in details. The transition probabilities per unit time for the solid-effect transitions are calculated. The double resonance spectra are calculated in the limiting cases of fast and slow nitrogen spin–lattice relaxation. The double resonance spectra are measured in histamine and quinolinic acid. The experimental spectra are analyzed and the ^{14}N NQR frequencies are determined.

1. Introduction

Nitrogen atoms are contained in a number of organic solids. The nuclear quadrupole interaction of the nitrogen nucleus ^{14}N is a sensitive tool for the investigation of the electric charge distribution around the nitrogen atom that is related to the molecular structure, intra and intermolecular interactions, etc.

In contrast to the half-integer-spin nuclei, as for example ^{17}O, the solid-state NMR of ^{14}N represents a difficult task. There is namely no central transition that is only slightly shifted from the Larmor frequency, while the width of the ^{14}N NMR lines in powders is typically a few MHz.

Pure nuclear quadrupole resonance (NQR) in zero magnetic field is usually used to determine the quadrupole coupling of ^{14}N. But the ^{14}N NQR frequencies are low and not known in advance. In addition the magnetic moment of a ^{14}N nucleus is small. The investigation of a broad frequency region thus represents a lengthy procedure.

Nuclear quadrupole double resonance (NQDR) with magnetic field cycling as introduced by Slusher and Hahn [1] represents an alternative that can be used to determine the low NQR frequencies in a short time. The resolution of NQDR is lower than the resolution of NQR, but when the NQR frequencies are approximately known it is easy to tune the NQR spectrometer in the appropriate frequency range and do the measurements of the NQR frequencies, spin–lattice relaxation rates, etc.

The main problem with ^{14}N is that it is an integer-spin nucleus ($S = 1$) that is in zero magnetic field decoupled from any other non-resonant nuclei [2]. The double resonance on the basis of magnetic field cycling and the application of the phase-modulated rf magnetic field [1] is in this case much less effective than in case of half-integer-spin nuclei. Various ^{1}H–^{14}N NQDR techniques based on magnetic field cycling [3–9] have been developed with the aim of increasing the sensitivity and resolution of the ^{14}N detection.

Strong rf magnetic field can in solid samples induce "forbidden transitions" at the sum or difference of the nuclear magnetic or quadrupole resonance frequencies. These transitions are called the solid-effect transitions and are allowed due to the internuclear dipole–dipole interaction. The solid-effect transitions in the system ^{1}H–^{35}Cl have been used in a study of the dynamic polarization of protons in paradichlorobenzene [10]. In that study the transition probabilities are calculated and measured as a function of rf power and d.c. field.

The situation is different in the system ^{1}H–^{14}N. The spin quenching effect [2] namely strongly reduces the proton–nitrogen dipolar interaction and decreases the transition probabilities. The double resonance technique based on the solid effect has already been applied to ^{14}N [5]. An analysis of the solid-effect double resonance in amino groups in zero magnetic field has also been performed [11].

In the present paper we calculate the transition probabilities per unit time for the solid-effect transitions in the system ^{1}H–^{14}N

* Corresponding author. Address: University of Ljubljana, Faculty of Mathematics and Physics, Department of Physics, Jadranska 19, 1000 Ljubljana, Slovenia. Fax: +386 1 2517281.
E-mail address: janez.seliger@fmf.uni-lj.si (J. Seliger).

1090-7807/$ - see front matter © 2008 Elsevier Inc. All rights reserved.
doi:10.1016/j.jmr.2008.04.020

in a weak static magnetic field. Further we analyze the ^{1}H–^{14}N double resonance technique under various experimental conditions. Finally we present the experimental solid-effect NQDR spectra of histamine and quinolinic acid, analyze the spectra and determine the ^{14}N NQR frequencies.

2. Theory

2.1. Transition probabilities

Here we consider a system of identical pairs of nuclei, ^{1}H and ^{14}N, in a solid sample subject to a weak static magnetic field B. We first calculate the matrix elements for the simultaneous (solid-effect) transitions in both spin systems, an then using the Fermi's golden rule the transition probabilities per unit time for the solid-effect transitions.

We denote the nuclear spin of ^{14}N by $\vec{S}$ and the nuclear spin of ^{1}H by $\vec{I}$. The approximate Hamiltonian for an arbitrary pair from our system is given as

$$H = H_{\mathrm{QN}} + H_{\mathrm{ZH}} + H_{\mathrm{DNH}}. \tag{1}$$

Here we neglect the weak Zeeman interaction of the ^{14}N nucleus. The reason is that the magnetic moment of a ^{14}N nucleus is small and also the magnetic field B is weak. We also neglect the dipolar interaction between the pairs of nuclei and the dipolar interaction of the given pair of nuclei with the rest of protons.

The quadrupole energy levels, eigenstates and transition frequencies of a ^{14}N nucleus are presented in Fig. 1. The quantization axis is the z-principal axis of the electric-field-gradient (EFG) tensor at the position of the ^{14}N nucleus. The nonzero matrix elements of the ^{14}N nuclear spin $\vec{S}$ between the quadrupole eigenstates are: $\langle a|S_x|c\rangle = \langle c|S_x|a\rangle = \langle a|S_z|b\rangle = \langle b|S_z|a\rangle = 1$ and $\langle b|S_y|c\rangle = \langle c|S_y|b\rangle^* = -i$. Here x, y, and z are the principal axes of the EFG tensor corresponding to the smallest, intermediate and the largest principal value, respectively.

The proton Zeeman Hamiltonian is $H_{\mathrm{ZH}} = -h\nu_{\mathrm{L}} I_{z'}$. Here ν_{L}, $\nu_{\mathrm{L}} = \gamma B/2\pi$, is the proton Larmor frequency in the low magnetic field B and z' represents the direction of the magnetic field B. The eigenstates of H_{ZH} are denoted as $|-\rangle$ and $|+\rangle$, and the energy difference $E_- - E_+$ is equal $h\nu_{\mathrm{L}}$.

The proton–nitrogen dipolar interaction term that is responsible for the nonzero probability of the solid-effect transitions is

$$H_{\mathrm{DNH}} = \frac{\mu_0 \hbar^2 \gamma_{\mathrm{N}} \gamma_{\mathrm{H}}}{4\pi r^3}(\vec{S}\vec{I} - 3(\vec{S}\vec{n})(\vec{I}\vec{n})) = h\nu_{\mathrm{D}}(S_x O_x + S_y O_y + S_z O_z). \tag{2}$$

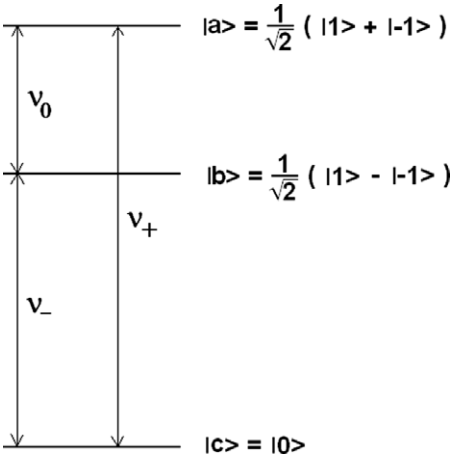

Fig. 1. Nuclear quadrupole energy levels, eigenstates and resonance frequencies of ^{14}N.

Here r is the distance between the nitrogen nucleus and proton, $\vec{n} = \vec{r}/r$ is the unit vector along the N–H direction, $\nu_{\mathrm{D}} = \mu_0 \hbar \gamma_{\mathrm{N}} \gamma_{\mathrm{H}}/8\pi^2 r^3 = 8.7\ \mathrm{kHz}/r^3\ (\text{Å})$, and the operators O_x, O_y and O_z are given as:

$$O_i = I_i - 3n_i(\vec{I}\vec{n}), \quad i = x, y, z. \tag{3}$$

The energy level diagram of a dipolarly coupled N–H pair and the possible solid-effect transitions are presented in Fig. 2. The state $|1\rangle$ is in case of no dipolar interaction ($H_{\mathrm{DNH}} = 0$) written in the product space as $|1\rangle = |a, -\rangle$, etc. The dipolar term H_{DNH} can be treated as a perturbation. In the first order perturbation theory for the eigenstates we obtain

$$\begin{aligned}
|1\rangle &= |a,-\rangle + \frac{\nu_{\mathrm{D}}}{\nu_0} O_z^{--}|b,-\rangle + \frac{\nu_{\mathrm{D}}}{\nu_0+\nu_{\mathrm{L}}} O_z^{+-}|b,+\rangle + \frac{\nu_{\mathrm{D}}}{\nu_+} O_x^{--}|c,-\rangle \\
&\quad + \frac{\nu_{\mathrm{D}}}{\nu_+ + \nu_{\mathrm{L}}} O_x^{+-}|c,+\rangle \\
|2\rangle &= |a,+\rangle + \frac{\nu_{\mathrm{D}}}{\nu_0-\nu_{\mathrm{L}}} O_z^{-+}|b,-\rangle + \frac{\nu_{\mathrm{D}}}{\nu_0} O_z^{++}|b,+\rangle + \frac{\nu_{\mathrm{D}}}{\nu_+ - \nu_{\mathrm{L}}} O_x^{-+}|c,-\rangle \\
&\quad + \frac{\nu_{\mathrm{D}}}{\nu_+} O_x^{++}|c,+\rangle \\
|3\rangle &= |b,-\rangle - \frac{\nu_{\mathrm{D}}}{\nu_0} O_z^{--}|a,-\rangle + \frac{\nu_{\mathrm{D}}}{\nu_0-\nu_{\mathrm{L}}} O_z^{+-}|a,+\rangle + i\frac{\nu_{\mathrm{D}}}{\nu_-} O_y^{--}|c,-\rangle \\
&\quad + i\frac{\nu_{\mathrm{D}}}{\nu_- + \nu_{\mathrm{L}}} O_y^{+-}|c,+\rangle \\
|4\rangle &= |b,+\rangle - \frac{\nu_{\mathrm{D}}}{\nu_0+\nu_{\mathrm{L}}} O_z^{-+}|a,-\rangle - \frac{\nu_{\mathrm{D}}}{\nu_0} O_z^{++}|a,+\rangle + i\frac{\nu_{\mathrm{D}}}{\nu_- - \nu_{\mathrm{L}}} O_y^{-+}|c,-\rangle \\
&\quad + i\frac{\nu_{\mathrm{D}}}{\nu_-} O_y^{++}|c,+\rangle \\
|5\rangle &= |c,-\rangle - \frac{\nu_{\mathrm{D}}}{\nu_+} O_x^{--}|a,-\rangle - \frac{\nu_{\mathrm{D}}}{\nu_+ - \nu_{\mathrm{L}}} O_x^{+-}|a,+\rangle + i\frac{\nu_{\mathrm{D}}}{\nu_-} O_y^{--}|b,-\rangle \\
&\quad + i\frac{\nu_{\mathrm{D}}}{\nu_- - \nu_{\mathrm{L}}} O_y^{+-}|b,+\rangle \\
|6\rangle &= |c,+\rangle - \frac{\nu_{\mathrm{D}}}{\nu_+ + \nu_{\mathrm{L}}} O_x^{-+}|a,-\rangle - \frac{\nu_{\mathrm{D}}}{\nu_+} O_x^{++}|a,+\rangle + i\frac{\nu_{\mathrm{D}}}{\nu_- + \nu_{\mathrm{L}}} O_y^{-+}|b,-\rangle \\
&\quad + i\frac{\nu_{\mathrm{D}}}{\nu_-} O_y^{++}|b,+\rangle
\end{aligned} \tag{4}$$

Here $O_\alpha^{\beta\gamma} = \langle\beta|O_\alpha|\gamma\rangle$.

Consider for example the solid-effect transitions 1–4 at the frequency $\nu_0 + \nu_{\mathrm{L}}$. We assume that an rf magnetic field with the frequency $\nu_0 + \nu_{\mathrm{L}}$ and amplitude B_1 is directed along a direction x' that is perpendicular to the direction z' of the static magnetic field B. The additional term H_{rf} in the Hamiltonian is in this case

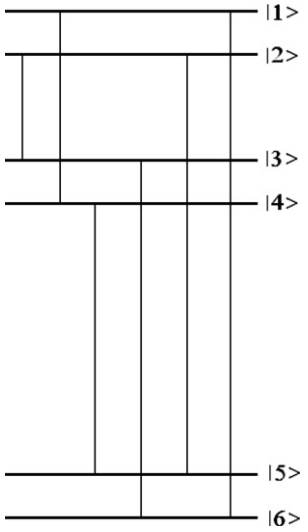

Fig. 2. Energy levels and the six possible solid-effect transitions of a dipolarly coupled ^{1}H–^{14}N pair.

$$H_{rf} = -(\hbar\gamma_N B_1 S_{x'} + \hbar\gamma_H B_1 I_{x'})\cos((\omega_0+\omega_L)t)$$
$$= -(h\nu_{1N}S_{x'} + h\nu_{1H}I_{x'})\cos((\omega_0+\omega_L)t). \quad (5)$$

Here $\nu_{1H} \approx 14\nu_{1N}$. The matrix element for this transition,

$$M_{1,4} = \langle 1| - (h\nu_{1N}S_{x'} + h\nu_{1H}I_{x'})|4\rangle, \quad (6)$$

may be due to the large value of ν_{1H} as compared to ν_{1N} expressed as

$$M_{1,4} \approx \langle a,-|h\nu_{1H}\frac{\nu_D}{\nu_0}I_{x'}O_z^{++}|a,+\rangle - \langle b,-|h\nu_{1H}\frac{\nu_D}{\nu_0}I_{x'}O_z^{--}|b,+\rangle$$
$$= h\nu_{1H}\frac{\nu_D}{\nu_0}(O_z^{++} - O_z^{--})\langle -|I_{x'}|+\rangle. \quad (7)$$

Here $\langle -|I_{x'}|+\rangle = 1/2$. If we further describe the orientation of the static magnetic field B in the principal-axes frame of the EFG tensor with the polar angle θ and azimuthal angle φ, we obtain

$$O_z^{++} = -O_z^{--}$$
$$= \frac{1}{2}\left[(1-3n_z^2)\cos\theta - 3n_xn_z\sin\theta\cos\varphi - 3n_yn_z\sin\theta\sin\varphi\right]. \quad (8)$$

The transition probability per unit time for this solid-effect transition, $W_{1,4}$, can be calculated using the Fermi's golden rule:

$$W_{1,4} = \frac{2\pi}{\hbar}|M_{1,4}|^2\rho(E) \approx \frac{2\pi}{\hbar}|M_{1,4}|^2\frac{1}{h\delta\nu_H}. \quad (9)$$

Here the density of final states $\rho(E)$ is approximated by $1/h\delta\nu_H$, where $\delta\nu_H$ is the width of the proton NMR line. Inserting Eqs. (7) and (8) into Eq. (9) we obtain

$$W_{1,4} \approx \frac{\pi^2\nu_{1H}^2\nu_D^2}{\nu_0^2\delta\nu_H}\left[(1-3n_z^2)\cos\theta - 3n_xn_z\sin\theta\cos\varphi - 3n_yn_z\sin\theta\sin\varphi\right]^2. \quad (10)$$

In practice we are dealing with the powder samples, where the orientation of the principal-axes frames is isotropically distributed. The transition probability per unit time varies with varying orientation of the principal axes of the EFG tensor with respect to the orientation of the static magnetic field. As an approximation of the transition probability per unit time we take the average over all possible orientations. We obtain:

$$\langle W_{1,4}\rangle \approx \frac{\pi^2\nu_{1H}^2\nu_D^2}{3\nu_0^2\delta\nu_H}(1+3n_z^2). \quad (11)$$

The largest average transition probability is obtained when the N–H bond is parallel to the principal axis z ($n_z = 1$). When the N–H bond is perpendicular to the principal axis z ($n_z = 0$) we obtain a four times smaller average transition probability per unit time.

By a similar calculation we obtain the average transition probabilities per unit time for the other five solid-effect transitions. The results are as follows:

$$\langle W_{2,3}\rangle = \langle W_{1,4}\rangle \approx \frac{\pi^2\nu_{1H}^2\nu_D^2}{3\nu_0^2\delta\nu_H}(1+3n_z^2)$$
$$\langle W_{4,5}\rangle = \langle W_{3,6}\rangle \approx \frac{\pi^2\nu_{1H}^2\nu_D^2}{3\nu_-^2\delta\nu_H}(1+3n_y^2) \quad (12)$$
$$\langle W_{2,5}\rangle = \langle W_{1,6}\rangle \approx \frac{\pi^2\nu_{1H}^2\nu_D^2}{3\nu_+^2\delta\nu_H}(1+3n_x^2)$$

In contrast to the transition probabilities per unit time in the system ^{1}H–^{35}Cl [10], the average transition probabilities per unit time in the present case depend on the NQR frequencies (ν_+, ν_-, ν_0), and not on the proton Larmor frequency ν_L. This is the consequence of the spin quenching effect [2]. In a typical case when $\nu_{1H} = 20$ kHz, $r = 1$ Å, $\nu_Q = 1$ MHz and $\delta\nu_H = 20$ kHz we obtain $\langle W\rangle \sim 15\ s^{-1}$. This transition probability per unit time is lower than the transition probability per unit time for the flip-flop transition in case of resonant coupling at $\nu_L = \nu_0$ [12], but it is high enough to perform a double resonance experiment.

2.2. Double resonance

A double resonance cycle is schematically presented in Fig. 3. The proton spin system is polarized in a high static magnetic field B_0 and then the static magnetic field is adiabatically reduced to a low value B. During the demagnetization process the separation of the proton energy levels decreases, but the population of the proton energy levels remains constant. It may change when the proton Larmor frequency crosses a ^{14}N NQR frequency [3]. The process is called level crossing. In a fast-field cycling spectrometer, where the field cycling is done electronically, the level crossing process is usually ineffective due to the fast reduction of magnetic field. When the magnetic field cycling is done by a slower mechanical motion between two magnets, the level crossing process is effective when the ^{1}H–^{14}N dipolar interaction is strong, i.e., in the case when also the solid-effect transition probabilities per unit time are not small.

The sample remains in the low magnetic field B for a time τ that is shorter than the proton spin–lattice relaxation time in the low magnetic field $T_{1H}(B)$. During this time we apply a strong rf magnetic field with the frequency ν. When ν is equal to a solid-effect frequency the rf magnetic field induces simultaneous transitions in the proton and ^{14}N spin systems that change the proton magnetization.

After the time τ the magnetic field is adiabatically increased to the initial value B_0 and the proton NMR signal $S(\nu)$ is measured immediately after the magnetic field B_0 is reached. It is proportional to the remaining proton magnetization.

In search of the ^{14}N NQR frequencies the above cycles are repeated at different frequencies ν of the rf magnetic field. The scan is usually performed in steps of 5–10 kHz. In the ν-dependence of the proton NMR signal S(ν) we generally observe dips at the solid-effect frequencies, NQR frequencies, and also when ν is equal to the proton Larmor frequency $\nu_L = \gamma_H B/2\pi$ and some its low multiples.

In the calculation of the intensity of the solid-effect dips we consider only two limiting situations:

(a) fast nitrogen spin–lattice relaxation, and
(b) slow nitrogen spin–lattice relaxation and effective level crossing during the decrease and increase of the external magnetic field.

In practice, when the solid-effect dips are observed, the situation is usually not far from one of the two limiting situations.

Let's denote the populations of the ^{14}N and proton energy levels in the low magnetic field B as shown in Fig. 4. Here N is one third of the number $N(N)$ of chemically equivalent nitrogen atoms and n is one half of the number $N(H)$ of protons in the sample. The deviations x, y, and z from complete disorder are small as compared to 1. The initial value of z is approximately $\nabla\gamma_H B_0/2k_BT$. Here T is the temperature of the sample.

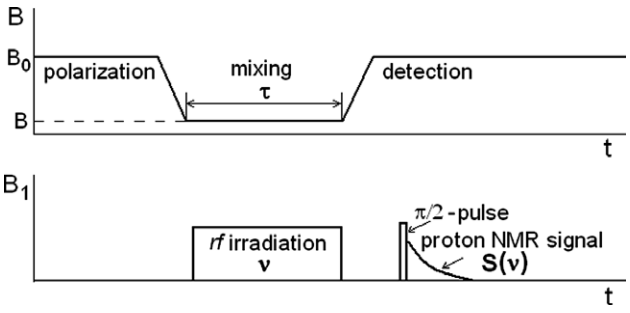

Fig. 3. Schematic presentation of a double resonance cycle.

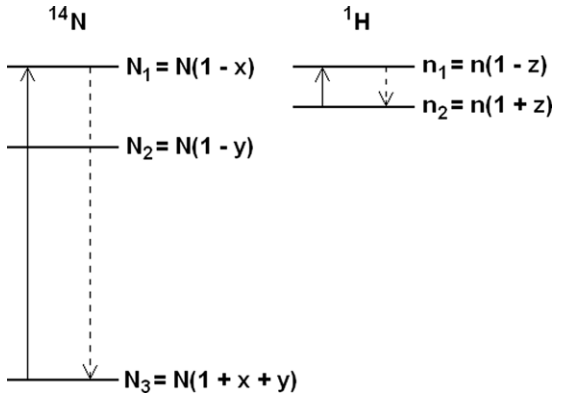

Fig. 4. Simultaneous solid-effect transitions in the dipolarly coupled ^{1}H–^{14}N system for the case $\nu = \nu_+ + \nu_L$ and the population of the energy levels.

The spin–lattice relaxation of nitrogen may be described by six transition probabilities per unit time as shown in Fig. 5. They are pairwise related as

$$\begin{aligned} W_i^{\uparrow} &= W_i(1 - \beta\hbar\omega_i/2) \\ W_i^{\downarrow} &= W_i(1 + \beta\hbar\omega_i/2) \end{aligned} \tag{13}$$

Here $i = 0, +, -$, and $\beta = 1/k_BT$. Also the spin–lattice relaxation of protons may be described by two transition probabilities per unit time, $W_H^{\uparrow}$ and $W_H^{\downarrow}$, where $W_H^{\uparrow} = W_H(1 - \beta\nabla\omega_L)$ and $W_H^{\downarrow} = W_H(1 + \beta\nabla\omega_L)$. The proton spin–lattice relaxation time in the low magnetic field B, $T_{1H}(B)$, is equal $T_{1H}(B) = (2W_H)^{-1}$. In most practical cases, when the proton Larmor frequency is in the high magnetic field B_0 large as compared to the highest ^{14}N NQR frequency ν_+, the difference between $W_i^{\uparrow}$ and $W_i^{\downarrow}$, $i = +, -, 0, H$, may be neglected. When this is not the case and especially if the solid-effect transitions are used to dynamically polarize protons, this difference must be taken into account.

The populations of the proton and nitrogen energy levels are in case of the solid-effect transitions at the frequency $\nu_+ + \nu_L$ governed during the mixing period by the following rate equations:

$$\begin{aligned} \frac{dN_1}{dt} &= -W_0^{\downarrow}N_1 - W_+^{\downarrow}N_1 + W_0^{\uparrow}N_2 + W_+^{\uparrow}N_3 - W_{1,6}N_1\frac{n_1}{2n} + W_{1,6}N_3\frac{n_2}{2n} \\ \frac{dN_2}{dt} &= -W_0^{\uparrow}N_2 - W_-^{\downarrow}N_2 + W_0^{\downarrow}N_1 + W_-^{\uparrow}N_3 \end{aligned}$$

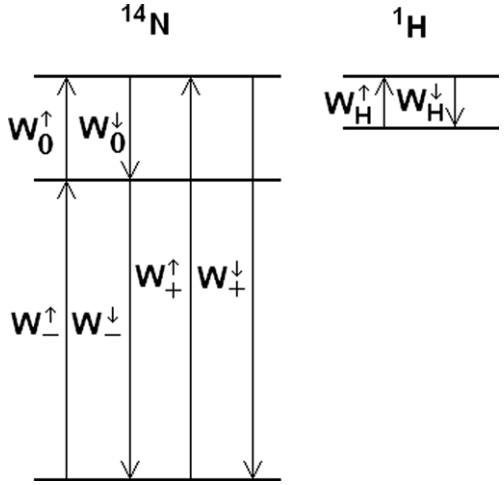

Fig. 5. Lattice-induced transition probabilities per unit time between the nitrogen and proton energy levels.

$$\begin{aligned} \frac{dN_3}{dt} &= -W_+^{\uparrow}N_3 - W_-^{\uparrow}N_3 + W_+^{\downarrow}N_1 + W_-^{\downarrow}N_3 + W_{1,6}N_1\frac{n_1}{2n} \\ &\quad - W_{1,6}N_3\frac{n_2}{2n}\cdot\frac{dn_1}{dt} = -W_H^{\downarrow}n_1 + W_H^{\uparrow}n_2 - W_{1,6}N_1\frac{n_1}{2n} + W_{1,6}N_3\frac{n_2}{2n} \\ \frac{dn_2}{dt} &= -W_H^{\uparrow}n_2 + W_H^{\downarrow}n_1 + W_{1,6}N_1\frac{n_1}{2n} - W_{1,6}N_3\frac{n_2}{2n} \end{aligned} \tag{14}$$

Here we assumed that $N(N) < N(H)$. These five equations are not independent. The populations of the proton and nitrogen energy levels is namely fully described by only three independent parameters x, y, and z ($x, y, z \ll 1$). Thus only three equations are independent. The above equations are valid when the frequency ν of the rf magnetic field is equal to $\nu = \nu_+ + \nu_L$. When a different solid-effect frequency, for example $\nu = \nu_- - \nu_L$, is hit by the rf magnetic field, the solid-effect terms in the rate equations change, whereas the spin–lattice relaxation terms remain the same.

The stationary solution of these equations for $t \to \infty$ gives the population of the energy levels of the two spin systems coupled via the solid-effect transitions and subject to the spin–lattice relaxation. The parameter z that is proportional to the proton magnetization is in case when $\nu = \nu_+ \pm \nu_L$ equal to

$$z = \frac{h\beta}{2}\frac{W_H[2W_Q^2 + W_{1,6}(W_- + W_0)]\nu_L \mp \varepsilon W_{1,6}W_Q^2\nu_+}{W_H[2W_Q^2 + W_{1,6}(W_- + W_0)] + \varepsilon W_{1,6}W_Q^2}. \tag{15}$$

Here $W_Q^2 = W_+W_- + W_+W_0 + W_-W_0$ and $\varepsilon = N/n = 2N(N)/3N(H)$. The proton spin system is strongly dynamically polarized when $W_H\left[2W_Q^2 + W_{1,6}(W_- + W_0)\right] \ll \varepsilon W_{1,6}W_Q^2$. In such a case z approaches the value $z \to \mp h\beta\nu_+/2$, corresponding to the equilibrium proton magnetization at the Larmor frequency $\nu_L = \nu_+$. When $\nu = \nu_+ + \nu_L$ the magnetization of the dynamically polarized proton spin system points opposite to the direction of the external magnetic field B, whereas for $\nu = \nu_+ - \nu_L$ the static magnetic field B and the proton magnetization point in the same direction.

The expression for the stationary value of z in case of $\nu = \nu_- \pm \nu_L$ is obtained from Eq. (15) by the following transformation: $W_{1,6} \to W_{3,6}$, $\nu_+ \to \nu_-$, and $W_- + W_0 \to W_+ + W_0$. The general conclusions are the same.

In the analysis of a double resonance experiment we first assume the case of fast nitrogen spin–lattice relaxation as compared to the proton spin–lattice relaxation ($W_+, W_-, W_0 > W_H$). For the sake of simplicity we also assume that $\gamma_H B_0 \gg 2\pi\nu_+$. The final proton magnetization in the low magnetic field B obtained at long mixing times t is in this case much lower than the initial proton magnetization. We may in this case neglect the difference between the transition probability per unit time for the upward transitions and the transition probability per unit time for the downward transitions and approximate the final magnetization with zero. In addition we assume that $N(N) \ll N(H)$.

The proton magnetization is immediately after the adiabatic demagnetization is complete approximately equal to the equilibrium proton magnetization in the high magnetic field B_0 and the parameter z that is proportional to the proton magnetization is at that moment approximately $z(0) \approx \nabla\gamma_H B_0/2k_BT$. The parameters x and y are much smaller and may be approximated with $x(0) = y(0) = 0$. When the rf magnetic field is switched on, the solid-effect transitions take place. Let us consider in details the situation when $\nu = \nu_+ + \nu_L$. We do not search the solution of Eq. (14) in general, but assume a situation where the solid effect transition probability per unit time $W_{1,6}$ is larger than W_+, W_-, and W_0. In such a simplified situation the solid-effect transitions first lead to a quasi-equilibrium in the coupled proton–nitrogen spin system with $N_1n_1 = N_3n_2$. Then the population of the nitrogen energy level that is not hit by the solid-effect transitions, N_2 in the present case, reaches a quasi-equilibrium value in a time that is short as com-

pared to the proton spin–lattice relaxation time. Finally the coupled spin systems relax towards the state of nearly complete disorder. The situation is illustrated in Fig. 6. The situation at the beginning of the mixing period, before the rf magnetic field is switched on, is illustrated in Fig. 6a. The quasi-equilibrium due to the solid-effect transitions is illustrated in Fig. 6b. Here $z' = zn/(n+N) \approx z$. The internal quasi-equilibrium in the nitrogen spin system due to the fast nitrogen spin–lattice relaxation and the simultaneous solid-effect transitions is illustrated in Fig. 6c. Here the relation between y'' and z'',

$$y'' = \frac{W_- - W_0}{3(W_- + W_0)} z'', \tag{16}$$

is calculated from Eq. (14) taking into account the above assumptions and putting $dN_2/dt = 0$. After the quasi-equilibrium (Fig. 6c) is reached the population of the proton and nitrogen energy levels depend on a single parameter (z'') which relaxes towards the new equilibrium value ($z'' \approx 0$) due to the proton and nitrogen spin–lattice relaxation. The relaxation time is obtained by summing expressions for dN_1/dt and dn_2/dt. In this sum namely the solid-effect terms subtract. Taking into account the above assumptions we may write

$$\frac{dN_1}{dt} + \frac{dn_2}{dt} \approx -W_0(N_1 - N_2) - W_+(N_1 - N_3) - W_H(n_2 - n_1). \tag{17}$$

Inserting into Eq. (17) the population of the energy levels (Fig. 6c) and assuming the relation between y'' and z'' as given by Eq. (16) we obtain a simple equation for z'',

$$\frac{dz''}{dt} = -Wz'', \tag{18}$$

where

$$W \cong 2W_H + \frac{N}{n}\left(2W_+ + 2\frac{W_- W_0}{W_- + W_0}\right) = 2W_H + 2\varepsilon W_N. \tag{19}$$

Here $\varepsilon = N/n$. The proton magnetization is proportional to z''. It thus relaxes towards zero with the relaxation rate W. Eq. (9) is valid when $N \ll n$ and $(N/n)W_N \geqslant W_H$, but it can be used as an approximate expression also when the two conditions are not strictly fulfilled.

When $N \ll n$ we may neglect the change of the proton magnetization during the setup of internal equilibrium (Fig. 6a–c). We assume that the internal equilibrium sets up in a time much shorter than τ. After a time τ, when the rf magnetic field is switched off, the proton magnetization is equal to $M(\tau) = M_0 \exp(-W\tau)$. If the rf magnetic field is not applied, the proton magnetization is at the same time equal $M_0(\tau) = M_0 \exp(-2W_H\tau)$. Here M_0 is the initial proton magnetization which is for $N \ll n$ approximately equal in both cases. The maximum difference $\Delta M(\tau) = M_0(t) - M(\tau)$ is obtained at the time

$$\tau = \frac{1}{2\varepsilon W_N} \ln\left(1 + \frac{\varepsilon W_N}{W_H}\right). \tag{20}$$

The relative change of the proton magnetization $\Delta M(\tau)/M_0(\tau)$ is at this time equal

$$\frac{\Delta M(\tau)}{M_0(\tau)} = \frac{\varepsilon W_N}{W_H + \varepsilon W_N}. \tag{21}$$

The optimum time of detection is in case when $\varepsilon W_N < W_H$ equal to $\tau \cong (2W_H)^{-1} = T_{1H}(B)$. At a larger value of εW_N as compared to W_H we observe the maximum difference $\Delta M(\tau)$ at a shorter time τ.

The nitrogen contribution W_N to the spin–lattice relaxation rate W is for $\nu = \nu_+ - \nu_L$ equal as for $\nu = \nu_+ + \nu_L$. A symmetric solid-effect doublet is thus observed around the nitrogen NQR frequency ν_+ at the frequencies $\nu = \nu_+ \pm \nu_L$. Symmetric doublets are as well observed around the ^{14}N NQR frequencies ν_- and ν_0. The intensities of the three doublets are generally not the same. They namely depend on the nitrogen contribution W_N to the spin–lattice relaxation rate W, that is for $\nu = \nu_+ \pm \nu_L$ given by Eq. (19). The value of W_N is for $\nu = \nu_- \pm \nu_L$ and $\nu = \nu_0 \pm \nu_L$ obtained from Eq. (19) by the cyclic permutation of indices.

The proton relaxation during the mixing period is in case when W_N exceeds the solid-effect transition probability per unit time $W_{i,j}$, determined by W_H and $W_{i,j}$ as

$$W = 2W_H + \varepsilon W_{i,j}.$$

A completely different situation arises when the nitrogen transition probabilities per unit time W_+, W_-, and W_0 are low as compared to W_H. In this case we measure the change of the proton magnetization that is due to the first step in the setup of the internal quasi-equilibrium of the two spin systems Fig. 6a → b. This change of the proton magnetization was neglected in the previous discussion. In addition the level crossings must be taken into account that occur during the increase and decrease of the external magnetic field. In the following discussion we shall assume that the level crossings are fully effective i. e. when the proton Larmor frequency ν_L matches a nitrogen NQR frequency ν_Q, the ratio of the populations of the two proton energy levels and the ratio of the population of the two nitrogen energy levels separated by $\nu_Q = \nu_L$ equalize. The lowest proton Larmor frequency, $\nu_L = \gamma_H B/2\pi$, is assumed to be lower than ν_0. In the following calculation we assume the time τ to be short as compared to $T_{1H}(B)$, and the ratio $\varepsilon = N/n$ to be small. We shall only calculate the change of the proton magnetization that is linear in $\varepsilon = N/n$. A more thorough analysis of the level crossings is given in Ref. [13].

The population of the proton and nitrogen energy levels at the beginning of the mixing period is to the lowest order in ε shown in Fig. 7a. The nitrogen spin system is polarized by the proton spin

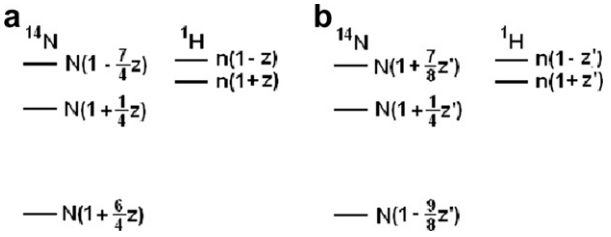

Fig. 7. Population of the proton and nitrogen energy levels immediately after the demagnetization is complete (a) and after the application of a pulse of the rf magnetic field at $\nu = \nu_+ + \nu_L$ (b).

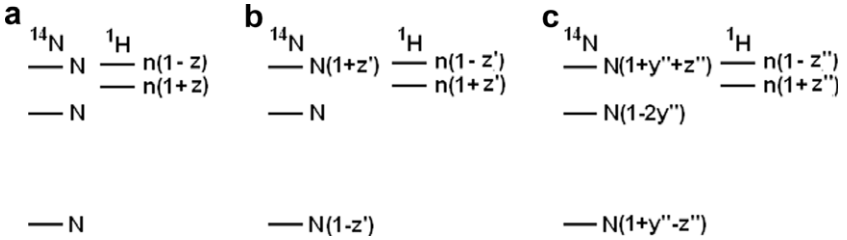

Fig. 6. Rearrangement of the population of the ^{14}N and ^{1}H energy levels after the rf magnetic field is switched on. The details of the process are described in the text.

system during the level crossings. The situation after the application of a pulse of the rf magnetic field at the frequency $\nu = \nu_+ + \nu_L$ is shown in Fig. 7b.

The parameter z at the beginning of the mixing period is to the first order in ε equal $z = z(0)(1 - 9\varepsilon/4)$. Here $z(0) = \nabla\gamma_H B_0/2k_BT$. The term $9\varepsilon/4$ is the consequence of the level crossings. If we describe the population of the nitrogen and proton energy levels with the parameters x, y, and z, as shown in Fig. 4, we obtain after the second set of level crossings the following parameter z'' that describes the population of the proton energy levels:

$$z'' = z[1 - \varepsilon(9z/4 - 13x/8 - 5y/8)]. \quad (22)$$

When no rf magnetic field is applied during the mixing period, we obtain after the second set of level crossings $z'' = z(0)(1 - 9\varepsilon/4 + 14\varepsilon/32)$.

When the rf magnetic field is applied during the mixing period the situation depends on whether its frequency ν hits a NQR frequency or a solid-effect frequency. In the former case the rf magnetic field equalizes the population of the corresponding two ^{14}N energy levels, while in the later case the setup of the quasi-equilibrium, as illustrated in Fig. 7b for the case $\nu = \nu_+ + \nu_L$, changes also the parameter z. The value of z' is for $\nu = \nu_+ + \nu_L$ equal $z' = z(1 - 21\varepsilon/8)$. In both cases the parameters x and y change as well. Taking into account this change of z we obtain after the second set of level crossing the parameter $z''(\nu)$. The relative change of the proton magnetization, that is due to the rf irradiation at the frequency ν, $\Delta M(\nu)/M$, may be expressed as

$$\Delta M(\nu)/M = (z'' - z''(\nu))/z'' \cong (z'' - z''(\nu))/z(0). \quad (23)$$

The ratio $\Delta M(\nu)/M$ is tabulated in Table 1. The situation is illustrated in Fig. 8. The most intensive line is observed at $\nu = \nu_+ + \nu_L$. The lines at the frequencies ν_+, $\nu_- + \nu_L$, $\nu_0 + \nu_L$, and ν_0 are weaker, but are usually observed. The weak lines at the frequencies $\nu_+ - \nu_L$, ν_-, $\nu_- - \nu_L$, and $\nu_0 - \nu_L$ are often not observed.

It should be mentioned once again that the intensities of the double resonance lines are calculated in the linear approximation. In practice ε is often not much less than one and the higher orders in ε must be taken into account. Also the spin–lattice relaxation of nitrogen may not be always neglected. Thus the asymmetry of the solid-effect doublet around a NQR frequency is in practice lower than shown in Fig. 8, but in most cases the five most intensive lines shown in the same figure are also in practice the most intensive.

3. Experimental

In order to demonstrate the application of the above described technique for the determination of the ^{14}N NQR frequencies in nitrogen containing solids we measured the ^{14}N NQR frequencies in solid quinolinic acid and histamine. The molecules are shown in Fig. 9.

In quinolinic acid there is a single nitrogen position in the molecule and the parameter ε is $\varepsilon = 2/15 \ll < 1$. The linear approximation as used in the analysis of the double resonance experiment is thus a good approximation. The solid-effect spectra are recorded at $\nu_L = 90$ kHz and $\nu_L = 50$ kHz under the following experimental conditions. The temperature of the sample is 22 °C, the polarization time in $B_0 = 0.75$ T is 60 s, the mixing time is $\tau = 1$ s, and the amplitude of the rf magnetic field is approximately 3 mT. A commercially available sample is used. The results are presented in Fig. 10. Besides the direct proton absorption lines in the low-frequency part of the spectra there are also the lines corresponding to the solid-effect and direct NQR transitions. These lines are indicated by arrows. The triplet centered at $\nu = \nu_+ = 880$ kHz shows the direct NQR transition and the solid-effect transitions at $\nu = \nu_+ \pm \nu_L$. In the low-frequency part of the spectra there are four lines observed. The NQR lines at $\nu = \nu_0 = 390$ kHz and $\nu = \nu_- = 490$ kHz as well as the solid-effect lines at $\nu = \nu_0 + \nu_L$ and $\nu = \nu_- + \nu_L$. The spectra clearly indicate that the spin–lattice relaxation rates of ^{14}N are low as compared to $1/\tau$.

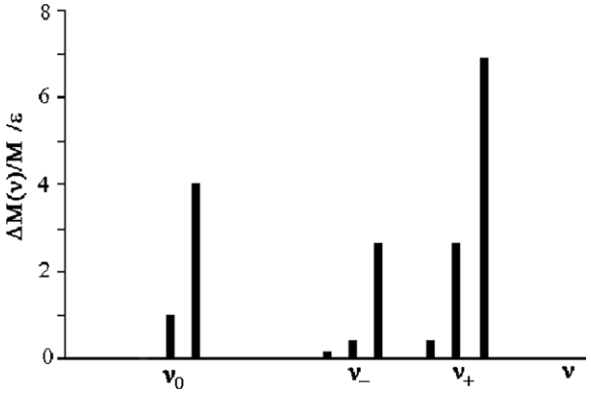

Fig. 8. The intensities of the ^{1}H–^{14}N double resonance lines in case of slow nitrogen spin–lattice relaxation.

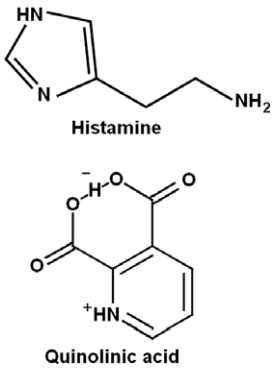

Fig. 9. Chemical structures of histamine and quinolinic acid in the solid phase.

The quadrupole coupling constant of ^{14}N is $e^2qQ/h = 910$ kHz and the asymmetry parameter is $\eta = 0.85$. These data clearly indicate [14,15] that the ring nitrogen is protonated in agreement with the neutron diffraction data [16] which show that in the solid phase the two carboxyl groups donate one hydrogen to the ring nitrogen, while the other hydrogen participates in a strong nearly symmetric intramolecular hydrogen bond.

In histamine there are three nonequivalent nitrogen positions in the molecule. The parameter ε is for each nitrogen position equal $\varepsilon = 2/27$. Two nitrogen positions, NH and NH_2, are suitable for the solid-effect. Some double resonance lines from the third nitrogen position, *N*, may not appear in the spectrum.

The experiment is performed at $T = -50$ °C and the spectrum is shown in Fig. 11. The proton polarization time in $B_0 = 0.75$ T is 10 s and the mixing time is $\tau = 0.35$ s. The proton Larmor frequency in the low magnetic field B is $\nu_L = 200$ kHz. The amplitude of the rf

Table 1
The intensities of the double resonance lines in case of slow nitrogen spin–lattice relaxation

ν	$\nu_+ + \nu_L$	ν_+	$\nu_+ - \nu_L$	$\nu_- + \nu_L$	ν_-	$\nu_- - \nu_L$	$\nu_0 + \nu_L$	ν_0	$\nu_0 - \nu_L$
$\Delta M(\nu)/M/\varepsilon$	441/64	169/64	25/64	169/64	25/64	9/64	4	1	0

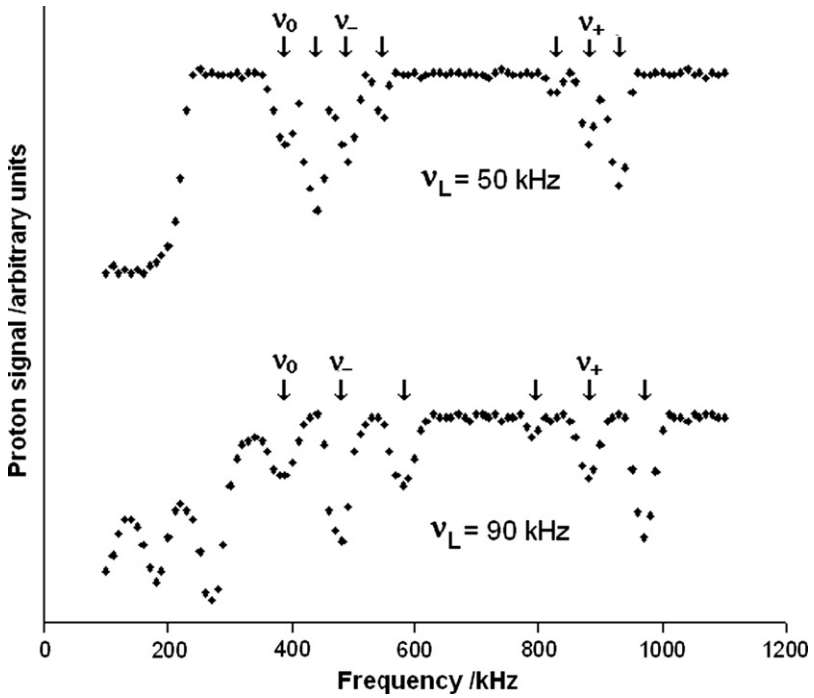

Fig. 10. NQDR spectra of quinolinic acid. The direct NQR transitions and the solid-effect transitions are indicated by arrows. The NQR transitions are labeled.

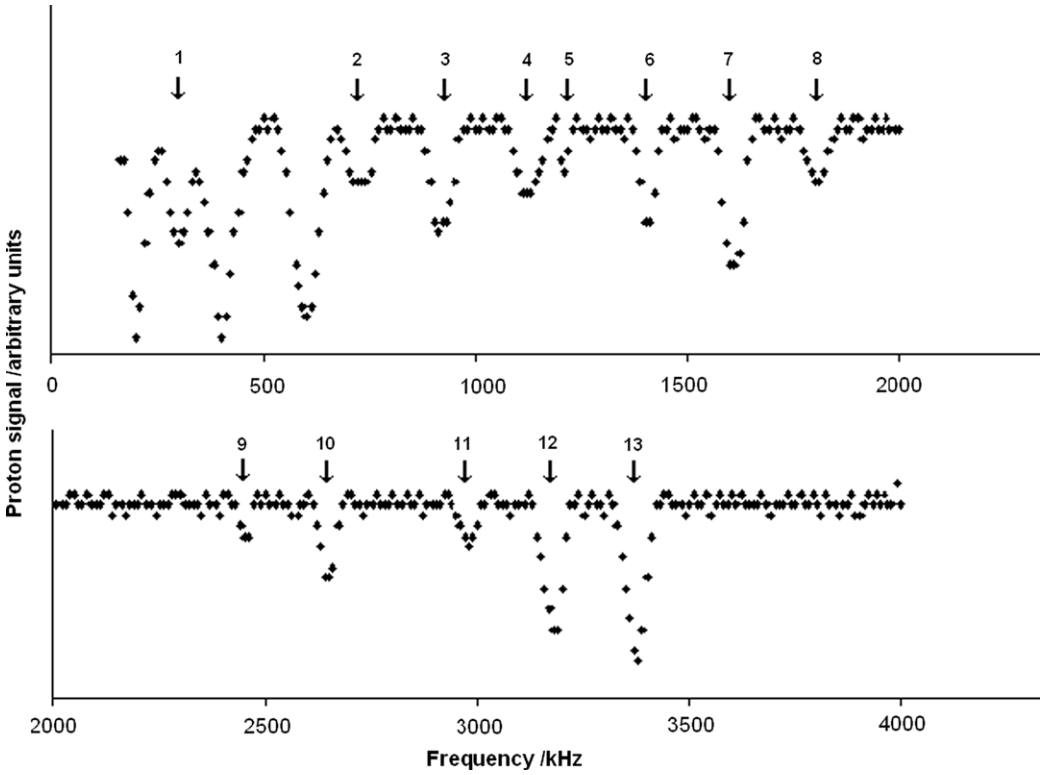

Fig. 11. NQDR spectrum of histamine. The direct NQR transitions and the solid-effect transitions are indicated by arrows and numbered.

magnetic field is approximately 3 mT for $\nu < 1$ MHz and approximately 6 mT for $\nu > 1$ MHz. A commercially available sample is used. The three strong lines observed at 200, 400, and 600 kHz correspond to the direct saturation of the proton system at $\nu = \nu_L$, $2\nu_L$, and $3\nu_L$. The triplet of the lines 11, 12, and 13 shows the two solid-effect transitions (11 and 13) and the direct transition (12) at the NQR frequency ν_+ of the nitrogen at the NH_2 position. The direct transition 9 at $\nu = \nu_-$ and the solid-effect transition 10 at $\nu = \nu_- + \nu_L$ correspond to the same nitrogen. Here the line at the frequency $\nu = \nu_- - \nu_L$ is not observed. The situation is much more complicated in the low-frequency part of the spectrum. The lines 5, 6, 7, and 8 correspond to $\nu = \nu_+ - \nu_L$, ν_+, $\nu_+ + \nu_L$ and $\nu_+ + 2\nu_L$ of the ring nitrogen NH. The line at $\nu_+ + 2\nu_L$ may be observed when the proton–proton dipolar interaction is strong. In the present case this is presumably

Table 2
^{14}N NQR frequencies, quadrupole coupling constants and asymmetry parameters η in histamine at $T = -50$ °C

Nitrogen position	ν_+/kHz	ν_-/kHz	ν_0/kHz	e^2qQ/h/kHz	η
NH_2	3180	2445	735	3750	0.392
NH	1410	705	705	1410	1.00
N	2675	2560	115	3490	0.066

the dipolar interaction of the three ring protons. Measurement of the position of the line 8 at different ν_L is used to confirm that it is indeed the solid-effect line at $\nu = \nu_+ + 2\nu_L$. The line 2 contains three NQR lines: the lines at the frequencies ν_- and ν_0 of the ring nitrogen NH that are equal within the experimental resolution and the line at the frequency ν_0 of the nitrogen at the NH_2 position. The lines 3 and 4 are the solid-effect lines corresponding to the NQR lines within the line 2. The line 4 is again observed at $\nu_Q + 2\nu_L$. The line 1 is the solid-effect line at the frequency $\nu_0 + \nu_L$ of the ring nitrogen N. This is confirmed by observing its position at different ν_L and later by the two-frequency irradiation. The high-frequency NQR lines of the ring nitrogen N are not observed by this technique.

The above spectrum clearly shows that the solid-effect technique gives the location of the low-frequency ^{14}N NQR lines and also the location of some high-frequency lines. The two-frequency irradiation technique [8], the two-frequency solid-effect technique [17] and the application of multiple frequency sweeps [9] can be on the basis of the solid-effect data used to improve the resolution and sensitivity and to find the lines that may be missing in the solid-effect and level crossing spectra. In the present case we use the two-frequency irradiation technique. The results are summarized in Table 2. The known ^{14}N NQR parameters of the imidazole ring [18,19] and of the amines [11,20] are used to assign the spectrum.

4. Conclusions

The transition probabilities per unit time are calculated for the solid-effect transitions in the system ^{1}H–^{14}N in a weak magnetic field. They are proportional to the square of the amplitude of the rf magnetic field, inversely proportional to the sixth power of the proton nitrogen distance and to the square of the corresponding ^{14}N NQR frequency. In addition they depend on the orientation of the N–H bond with respect to the principal axes of the EFG tensor. In contrast to the case of half-integer-spin quadrupole nuclei [10] the transition probabilities per unit time are nearly independent on the low d.c. magnetic field B.

The ^{14}N–^{1}H double resonance using the solid effect is analyzed in two limiting cases. When the spin–lattice relaxation of ^{14}N is fast we observe a nearly symmetric doublet around a NQR frequency with the intensity depending either on the nitrogen spin–lattice relaxation rate or on the transition probability per unit time for the solid-effect transition when the spin–lattice relaxation of ^{14}N is very fast. The solid-effect transitions may be used for the dynamic polarization of protons.

When the nitrogen spin–lattice relaxation is slow, a combination of lines corresponding to the solid-effect transitions and to the direct NQR transitions is observed. The intensity of the nine lines, that are in principle observed in a NQR experiment for a given nitrogen position, is calculated. The intensity strongly varies from line to line. Usually the solid-effect line at $\nu = \nu_+ + \nu_L$ is the strongest. Somewhat weaker are the lines at $\nu = \nu_+$, $\nu_- + \nu_L$, $\nu_0 + \nu_L$ and ν_0, whereas the weak lines at $\nu = \nu_-$, $\nu_- - \nu_L$ and $\nu_0 - \nu_L$ are often not observed.

The application of the solid-effect NQDR technique is demonstrated in cases of quinolinic acid with all nitrogen positions chemically equivalent and histamine where there are three chemically nonequivalent nitrogen positions per molecule. Both spectra are close to the ones expected in case of slow ^{14}N spin–lattice relaxation. In addition to the "normal" solid-effect lines we observed also some higher-order lines at the frequency $\nu = \nu_Q + 2\nu_L$ that may occur when the proton–proton dipole interaction is strong. In histamine these lines are associated with the nitrogen at the NH position in the imidazole ring. The strongly coupled protons are thus the nuclei of three ring hydrogens. In addition to the double resonance lines there are also the lines corresponding to the direct absorption of the proton spin system at its Larmor frequency and some of its low multiples. In histamine as well as in quinolinic acid these lines are observed at $\nu = \nu_L$, $2\nu_L$, and $3\nu_L$, what may again be associated with the nuclei of the strongly coupled ring hydrogens. Various double resonance spectra taken at different values of the low magnetic field B are in practice necessary for the proper assignment of the lines.

The ^{14}N NQR spectra, as determined by the present technique, may be in the next step refined by the two-frequency irradiation technique [8]. Also some lines that do not appear in the solid-effect spectrum may be observed by the two-frequency irradiation technique. In histamine these are the high-frequency lines from the ring nitrogen that is not directly bound to hydrogen.

The ^{1}H–^{14}N double resonance technique using the solid effect is thus a simple technique that can be used to gain information on the position of the low-frequency ^{14}N NQR lines and also some high-frequency lines in a short time. Its resolution is mainly determined by the proton NMR linewidth and is typically several kHz. NQDR using two-frequency irradiation or pure NQR techniques can be used in the second step to measure the ^{14}N NQR. frequencies with a higher precision and to determine some other parameters, like for example spin–lattice relaxation rates.

References

[1] R.E. Slusher, E.L. Hahn, Sensitive detection of nuclear quadrupole interactions in solids, Phys. Rev. 166 (1968) 332–347.
[2] G.W. Leppelmeier, E.L. Hahn, Nuclear dipole field quenching of integer spins, Phys. Rev. 141 (1966) 724–731.
[3] R. Blinc, M. Mali, R. Osredkar, A. Prelesnik, J. Seliger, I. Zupančič, L. Ehrenberg, ^{14}N NQR spectroscopy of some amino acids and nucleic bases via double resonance in the laboratory frame, J. Chem. Phys. 57 (1972) 5087–5093.
[4] D.T. Edmonds, Nuclear-quadrupole double-resonance, Phys. Rep. 29 (1977) 234–290.
[5] J. Seliger, R. Blinc, M. Mali, R. Osredkar, A. Prelesnik, Nuclear double resonance via the solid effect, Phys. Stat. Sol. (a) 25 (1974) K121–K123.
[6] J. Seliger, R. Blinc, M. Mali, R. Osredkar, A. Prelesnik, Nuclear magnetic double resonance based on strong rf magnetic-field-induced coupling between spin systems, Phys. Rev. B 11 (1975) 27–36.
[7] J. Seliger, R. Osredkar, M. Mali, R. Blinc, ^{14}N quadrupole resonance of some liquid crystalline compounds in the solid, J. Chem. Phys. 65 (1976) 2887–2891.
[8] J. Seliger, V. Žagar, R. Blinc, A new highly-sensitive ^{1}H–^{14}N nuclear-quadrupole double-resonance technique, J. Magn. Reson. A 106 (1994) 214–222.
[9] J. Seliger, V. Žagar, R. Blinc, ^{1}H–^{14}N Nuclear quadrupole double resonance with multiple frequency sweeps, Z. Naturforsch. 49a (1994) 31–34.
[10] A. Landesman, Polarisation dynamique en bas champ des protons du paradichlorobenzene, J. Phys. Chem. Solids 18 (1961) 210–214.
[11] S.V. Anferova, V.S. Grechishkin, G.V. Mozzhukin, Solid effect in double quadrupole resonance of nitrogen nuclei in amino groups, J. Struct. Chem. 27 (1986) 50–53.
[12] D.W. Prescott, O. Olmedo, S. Soon, K.L. Sauer, Low-field approach to double resonance in NQR of spin-1, J. Chem. Phys. 126 (2007) 204504.
[13] J. Lužnik, J. Pirnat, V. Jazbinšek, T. Apih, R. Blinc, J. Seliger, Improved ^{14}N nuclear quadrupole resonance detection of trinitrotoluene using polarization transfer from protons to ^{14}N nuclei, J. Appl. Phys. 102 (2007) 084903.
[14] G.V. Rubenacker, T.L. Brown, Nitrogen-14 nuclear quadrupole resonance spectra of coordinated pyridine. An extended evaluation of the coordinated nitrogen model, Inorg. Chem. 19 (1980) 392–398.
[15] J. Seliger, V. Žagar, A. Zidanšek, R. Blinc, ^{14}N nuclear quadrupole resonance of picolinic, nicotinic, isonicotinic and dinicotinic acids, Chem. Phys. 331 (2006) 131–136.
[16] A. Kvick, T.F. Koetzle, R. Thomas, F. Takusagawa, Hydrogen bond studies. 85. A very short, asymmetrical, intramolecular hydrogen bond: a neutron diffraction

study of pyridine-2,3-dicarboxylic acid ($C_7H_5NO_4$), J. Chem. Phys. 60 (1974) 3866–3874.
[17] J. Seliger, V. Žagar, A new nuclear-quadrupole double-resonance technique based on solid effect, Z. Naturforsch. 52a (1997) 337–342.
[18] J. Koo, Y.N. Hsieh, N-14 nuclear quadrupole coupling constants in imidazole, Chem. Phys. Lett. 9 (1971) 238–241.
[19] J.N. Latosinska, J. Seliger, B. Nogaj, Electron density distribution in 2-nitro-5-methylimidazole derivatives studied by NMR–NQR double resonance, Magn. Reson. Chem. 37 (1999) 878–880.
[20] R. Blinc, J. Seliger, A. Zidanšek, V. Žagar, F. Milia, H. Robert, ^{14}N nuclear quadrupole resonance of some sulfa drugs, Solid State Nucl. Magn. Reson. 30 (2006) 61–68.